Humidity dependence of anode corrosion in HERA-B Outer Tracker Chambers operated with $Ar/CF_4/CO_2$

A. Schreiner [a], G. Bohm [a], H. Kolanoski [b,*], M. Walter [a]

[a] *DESY Zeuthen, Germany*

[b] *Humboldt University, Berlin, Germany*

Presented by A. Schreiner

Abstract

The Outer Tracker of the HERA-B experiment consists of drift tubes folded from gold-coated polycarbonate foils (honeycomb) and is operated with the gas mixture $Ar/CF_4/CO_2$. The choice of the materials and the drift gas was the result of an extended R&D program launched to avoid both anode aging (gain loss) and cathode aging (Malter effect). However, other aging effects were observed at high irradiation doses: rising conductivity of the wire-supporting strips and wire corrosion. In this paper we show that these two aging effects could also be prevented by keeping water at a proper concentration (about 300 ppm). In an attempt to interpret the test results, the production and reaction probability of molecular species produced via CF_4 dissociation in the avalanche are semi-quantitatively estimated.

1 Introduction

The honeycomb chambers of the HERA-B Outer Tracker were designed to sustain an annual radiation dose of about 0.5 C/cm, thus comparable with that of similar tracking detectors in LHC experiments. This high radiation level demands extraordinary radiation resistance of the detectors. Extensive aging studies of the drift chambers led to substantial parameter changes in the design phase [1,2]. Aging tests of chambers with gold-coated polycarbonate cathode filled with $Ar/CF_4/CO_2$ (65:30:5) showed neither significant gain losses nor cathode aging, but revealed two new effects: radiation-induced dark

* Corresponding author: kolanoski@ifh.de

parameter	value
gas	$Ar/CF_4/CO_2$ (65:30:5)
gas pressure	1 bar
flow	1 vol/h
chambers	40 cm long honeycomb
cells	inner Ø=5 mm
cathode	75 μm Au/Cu-coated polycarbonate
anode	Au-plated tungsten wire Ø=25 μm
irradiation	X-rays (Mo at 35 kV)
Ø of irr. region	12 cm
HV	1750, 1800 V (intensity dependent)
gain	$6 \cdot 10^4$
current density	0.2, 0.4, 0.8 μA/cm
other materials	stainless steel, Al Stycast, Mylar, FR4

Table 1
Main working parameters of the aging test.

currents and anode corrosion. In this paper we show how these effects can be prevented. After a description of the tests and their results we try a theoretical interpretation by analyzing the plasma processes near the anode (see [3] for more details).

2 Experimental setup

In the aging tests described here, two identical chambers were simultaneously irradiated with an X-ray tube (Mo 35 kV). The chambers were constructed from folded gold-coated polycarbonate foil with a length of about 40 cm consisting of 14 cells with 5 mm inner diameter. In addition, they were equipped with 15 mm wide FR4 strips positioned symmetrically on both sides of the irradiated region, 10 cm from the chamber ends (not irradiated directly). The two chambers were placed vertically one after another in separate compart-

ments of an aluminum box (2.3 l) with aluminized Mylar windows towards the X-ray tube. The premixed gas mixture $Ar/CF_4/CO_2$ (65:30:5) with different water contents for different compartments flowed from a bottle to the input at the bottom of the boxes. Water was added by directing a fraction of the gas through a temperature-controlled ice box. The materials, the construction and the operation of the chambers were chosen as close as possible to those finally used for the Outer Tracker (table 1).

Measured parameters. We continuously recorded the currents for each irradiated wire and one reference wire (which was briefly connected to the high voltage for each measurement), the room temperature, the air pressure, and the temperature of the ice box. The dark currents were measured in regular intervals. The gas control system included "Panametrics" and "Hygrotec" hygrometers, as well as a "Teledyne" oxygen analyzer. A sensitivity down to about 10 ppm could be reached with the "Hygrotec" device employing a continuous calibration procedure where the zero point drift in particular was adjusted by calibrating with a dry gas in a reference bottle [4]. The precision of the moisture control was measured to be about 20% for the linearity and about 10 ppm for the offset.

3 Results

3.1 Wire corrosion

The chambers were irradiated for different humidity values of the drift gas. The most interesting observation was the rupture of anode wires after doses of typically 0.2 to 0.6 C/cm occurring always when the humidity was about 100 ppm or lower. Table 2 gives the water and oxygen contents at which tests were carried out and the doses after which the ruptures were observed. No strong dependence on the radiation intensity was observed [3]. Once the ruptures had started, most of the wires usually broke after a few 100 mC/cm additional radiation load. Ruptures always occurred in the centers of the irradiated regions of the cells. However, we did not observe any broken wire up to 4.5 C/cm when the humidity was approximately 350 ppm or higher. It should be noted that in [6] somewhat different results were obtained. The reason for the difference is not understood.

In order to understand the wire ruptures in dry gas, we investigated some of the damaged wires using Scanning Electron Microscopy (SEM) and Energy Dispersive X-ray Spectroscopy (EDS). The SEM micrographs and corresponding EDS spectra, as shown in Fig. 1, reveal that the wires ruptured due to corrosion. Organic deposits, typical for aging processes, were not observed. The

n	dose C/cm	H_2O in/out ppm	O_2 in/out ppm	onset of ruptures C/cm
rapid corrosion				
1	0.55	<10/50	30/200	0.3
2	1.2 (straws)	<10/100	30/200	0.6
3	1.2	<10/120	30/250	0.67
4	1	<10/<10	30/30	0.2
no corrosion				
5	4.5	350/400	30/200	never
6	3.5	700/750	30/300	never
7	1.5	350/400	30/30	never

Table 2
Observation of wire ruptures in X-ray tests at different humidity. Test 2 was done with straws of the ATLAS type [5].

surface of the wires upstream of the irradiated region was clean and undamaged. However, EDS spectra from the irradiated surface showed dominating W and sometimes O, C, and F. The dominance of the low energy line of W (1.7 keV) over the high energy line (9.7 keV) indicates that W is deposited above the gold layer. Near a rupture, the wire looked black under an optical microscope and a large part of the wire cross section was etched away. In this case (Fig.3b), we did not find a signal of species such as F, which could be responsible for anode corrosion: the W lines strongly dominated over the lines of C, O and Au in the EDS spectra.

In the process of irradiation, the wire diameter increased by several percent, as could be seen under the electron microscope on irradiated, but not yet ruptured wires. The swelling of the wires was followed by peeling off of the gold layer, which finally revealed tungsten. After 0.5 C/cm, we made longitudinal scans of the gain of several irradiated wires using an ^{55}Fe source. As can be seen in Fig. 2, the gain drops from the border of the irradiated region towards its center smoothly, reaching the minimum in the center of the irradiated region which is about 13% lower than in the non-irradiated part. The gain loss of 13% is consistent with the measurement of an increase in the wire diameter by about 1.3 μm (5%). The observed inhomogeneous distribution of gain losses could not be a result of an inhomogeneous irradiation intensity because the current density was measured to be uniform within a few percent in the irradiated area.

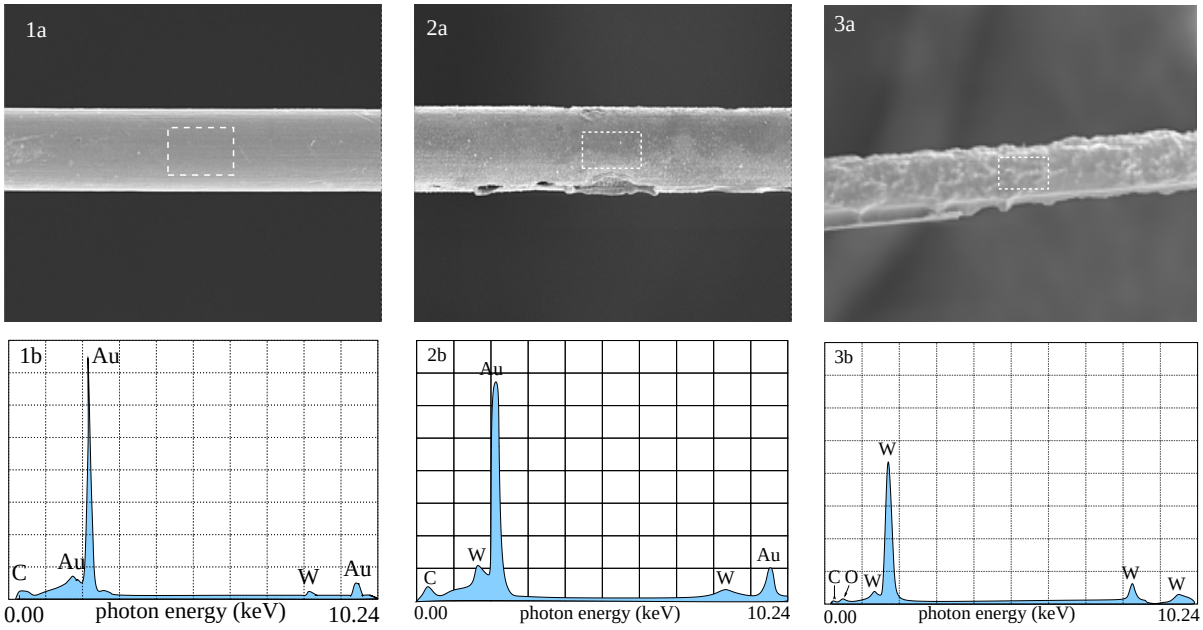

Fig. 1. 1a, 2a, 3a: SEM micrographs of some wires after a dose of 0.55 C/cm (see test 1 in table 2); 1b, 2b, 3b: EDS spectra from the area denoted by white rectangles on the corresponding upper micrographs. 1: a part of an irradiated wire upstream of the irradiated area; 2: a non-ruptured wire in the middle of the irradiated region; 3: a ruptured wire in the middle of the irradiated region.

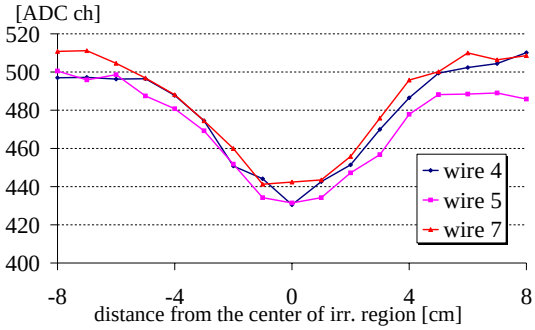

Fig. 2. Peak position of ^{55}Fe spectra along a wire relative to the center of the irradiated region.

A visual inspection of the cathodes of damaged chambers showed black deposits at the edges of the irradiated region which, according to EDS spectra, consisted of tungsten and smaller amounts of oxygen and carbon. It is likely that tungsten was also deposited inside the irradiated region but etched away by positive ions or radicals.

The FR4 strips near the irradiated region changed their appearance considerably: the surface of the strips had been etched away revealing the glass-fiber texture.

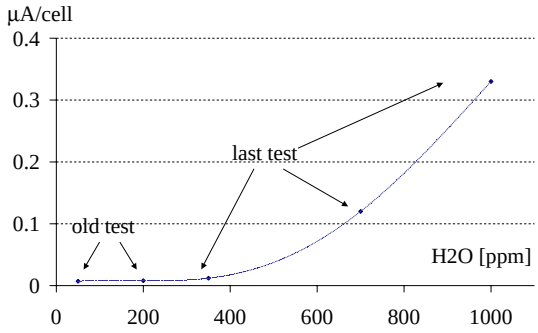

Fig. 3. Saturated dark current as a function of the water content in the drift gas.

3.2 Transient aging

Correlated to the observation of anode wire corrosion an effect, referred to as "transient aging", was observed: a temporary gain drop during high-rate operation which recovered during short irradiation breaks. This transient aging was considerably reduced when water was added in concentrations of more than 200 ppm or when the gas flow was increased. We interpret this effect to be caused by the very electronegative gas F_2 which is produced in the avalanche and reacts with H_2O.

3.3 Dark currents

During the first two weeks of irradiation (about 0.3 C/cm) the dark currents were continuously rising from around 100 pA at the beginning to a saturation level depending on the gas humidity and the irradiation intensity. In figure 3 the average saturated dark current in honeycomb chambers irradiated at the intensity of 0.6 μA/cm is plotted as a function of the gas humidity. The increase of the dark currents was analyzed to be caused by an increase of the FR4 strip conductivity under irradiation, which confirmed a previous observation of this effect[1]. Without irradiation the conductivity of the strips decreased to a negligible level after several months. In chambers made of straws of the ATLAS type, which did not have the FR4 strips and were operated under similar conditions, the dark currents were about three orders of magnitude lower than in honeycomb chambers.

4 Plasma chemistry in the avalanche in $Ar/CF_4/CO_2$

In the following we make an attempt to interpret the anode corrosion by developing a model for the plasma chemistry in the avalanche near the anode. Although plasma etching is well known from industrial applications, the mod-

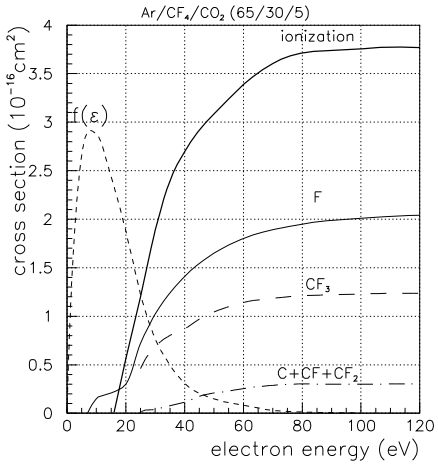

Fig. 4. Cross sections and energy distribution function (the latter in arbitrary units) as used in the calculation described in the text.

eling of drift chamber aging is difficult because unknown impurities from leaks and outgassing can play a significant role. As shown below, the presence of water drastically changes the outcome of plasma chemistry processes. Nevertheless, for the measured water and oxygen contents and with the assumption that the contents of the other impurities is insignificant, we estimated the concentration of products from the avalanche processes. These estimates can only serve as a guidance for understanding the aging results.

4.1 Production rate of fluorine species in $Ar/CF_4/CO_2$

The estimated cross sections describing the processes in the avalanche are shown in figure 4. According to [7], the cross sections for CO_2 electron-impact dissociation are rather small, more than one order of magnitude smaller than for CF_4 dissociation. Therefore, CO_2 dissociation was altogether neglected (although there could be other dissociation processes, for which we had insufficient information). The measured total ionization cross section for CF_4 was taken from [8], for argon and CO_2 from [9]. The molecule-averaged ionization cross section for the mixture $Ar/CF_4/CO_2$ (65:30:5) can be estimated as the percentage-weighted mean of the total ionization cross sections in pure gases. The cross sections for the production of fluorine by neutral dissociation and for the dissociative ionization by electron impact on CF_4 were measured in [10], for CF_3 in [8].

Nearly all the electrons are produced in the avalanche in a region within several microns from the anode wire. Fluorine and other free radicals are mainly produced in this region. The energy distribution function $f(\epsilon, r_a)$ of electrons

at the radius of the anode, r_a=12.5 μm, was calculated by the Magboltz program [11] and is also shown in Fig. 4. To simplify the calculation, we assume that the electric field, and hence $f(\epsilon)$, does not change significantly within a few microns. As shown in [3], the Magboltz program calculates the electron drift velocity in the region of low electric fields (rather remote from the anode) with a precision of a few percent. The program was also tested for the high electric field near the anode by comparing the calculated and measured Townsend coefficients. The prediction and the measurement agreed within a few 10% which is acceptable given the other uncertainties involved.

The approximate ratios for the production rates of free radicals to those of free electrons near the anode were calculated according to

$$\frac{\dot{N}_{r,prod}}{\dot{N}_{e,prod}} = \frac{\int \sigma_r f(\epsilon)\sqrt{\epsilon}\, d\epsilon}{\int \sigma_i f(\epsilon)\sqrt{\epsilon}\, d\epsilon}$$

yielding 0.6, 0.43 and 0.04 for F, CF_3 and the sum of C, CF and CF_2, respectively. The uncertainty of this calculation is dominated by the uncertainties of the given cross sections, which is estimated to be about 20%, and by the systematic uncertainties arising from considering only electron-impact dissociation. The latter are expected to be of a similar size as the contribution from impurities to the total ionization. Even a small concentration (several 100 ppm) of contaminant gases with a lower ionization potential can increase the ionization rate by several percent due to Penning processes, see e.g. [12]. In addition, an oxygen contamination could increase the fluorine production rate [13].

4.2 Lifetimes of species

As shown in the previous section, predominantly CF_3 and F are produced in the avalanche, near the anode. The total production rates of C, CF and CF_2 produced as neutral or charged species are lower by more than one order of magnitude. Let us simplify the multi-component reactions to a process with only two reacting components and a buffer gas (argon). In this case, the characteristic time constants calculated for different reactions are listed in table 3. The time constants are probably overestimated because it was not taken into account that radicals can also attach themselves to electrode surfaces, hence increasing the local density of radicals and providing the collision partner M in the three-body reaction processes (see table 3).

As can be seen in table 3, atomic fluorine reacts predominantly with water forming stable HF even if the water content is only 100 ppm. This semi-quantitative analysis indicates that fluorine is responsible for anode corrosion, since wire ruptures were never observed if water was added into the gas. With

Reaction	Const. [s]	Ref.
$CF_3+F+M \rightarrow CF_4+M$	0.1	[14]
$CF_3+CF_3+M \rightarrow C_2F_6+M$	0.046	[14]
$F+F+M \rightarrow F_2+M$	25 s	[15]
$H_2O+F \rightarrow HF+OH$	$2 \cdot 10^{-5}$	[15]
$F+O_2+M \rightarrow FO_2+M$	4	[15]
$F+CH_4 \rightarrow HF+CH_3$	$1.8 \cdot 10^{-9}$	[15]

Table 3
Characteristic time constants for possible reactions in a drift chamber with $Ar/CF_4/CO_2$ estimated for the current density of 0.6 μA/cm. In the three-body reactions Ar has been assumed as a quenching partner M. The water and oxygen contents in this estimation was assumed to be 100 ppm. The last reaction in the table is given to show the influence of CH_4 on the F lifetime in an $Ar/CF_4/CH_4$ (74:20:6) mixture.

sufficient water in the gas, HF is produced in the drift cell during the irradiation. HF itself is not very reactive, but together with water forms hydrofluoric acid. Hydrofluoric acid is weakly dissociated and thus electro-conductive. If HF is absorbed on the FR4 strips, it can cause the observed increase of the conductivity.

The strips recovered their original high resistivity within several months after stopping the irradiation almost completely (both in air and in the pure counting gas). This indicates that the conductivity is not a result of corrosion, which would cause a permanent effect, but could be explained by the dissociation into ions of the species which diffused into the strips. A study of the influence of hydrofluoric acid on the FR4 strip conductivity could prove this hypothesis.

5 Summary and conclusion

In aging tests of the HERA-B Outer Tracker honeycomb drift tubes with a gold-coated polycarbonate cathode using the gas mixture $Ar/CF_4/CO_2$ (65:30:5), wire ruptures were observed after an irradiation of approximately 0.3 C/cm when the water content was very low (about 100 ppm or lower). Under an electron microscope it could be seen that wires swelled (the diameters increased by several percent) and the gold-coating on the wires peeled off. An estimation of the plasma density near the anode suggests that atomic fluorine is responsible for anode corrosion. The observed humidity dependence supports this explanation.

Strong dark currents (>0.3 μA/cell) were observed in honeycomb chambers when the humidity of the gas was rather high (>500 ppm). These dark currents are specific for this type of honeycomb chambers since they are caused by an increased conductivity of the wire-supporting FR4 strips. The dark currents increased at the beginning of the irradiation and saturated typically after 0.3 C/cm. The effect can be explained by the production of HF which reacts with water forming weakly conductive hydrofluoric acid.

In conclusion, reliable operation of the Outer Tracker is expected for a controlled water content between 300 ppm and 500 ppm.

References

[1] H. Albrecht, et al., these proceedings.

[2] K. Berkhan et al., these proceedings.

[3] A. Schreiner, Ph.D. thesis, Humboldt University, Berlin (2001), http://www-hera-b.desy.de.

[4] A. Schreiner, Test of Devices with Capacity-Based Sensors for Measurement of Low Water Contents, HERA-B-01-135 (2001).

[5] ATLAS Collaboration, The ATLAS Technical Proposal for a general purpose pp experiment at the Large Hadron Collider at CERN, CERN/LHCC/94-43 (1994) 78.

[6] M. Capeans, et al., A long-term aging study of honeycomb drift tubes for the HERA-B Outer Tracker using a circulated and purified CF_4 mixture, these proceedings.

[7] L. Kieffer, A Compilation of Electron Collision Cross-Section Data for Modeling Gas Discharge Lasers, JILA COM-74–11661, Boulder, Colorado (1973).

[8] L. Cristophorou, et al., J. Phys. Chem. Ref. Data 25 (1996) 1341.

[9] I. Grigoriev, et al., Handbook of physical quantities, Kurchatov Institute, Moscow (1997).

[10] S. Motlagh, et al., J. Chem. Phys. 109 (1998) 432.

[11] S. Biagi, http://consult.cern.ch/writeup/magboltz/.

[12] L. Cristophorou, Atomic and Molecular Radiation Physics, Wiley (1971) 50.

[13] C. Mogab, J. Appl. Phys. 49 (1978) 3796.

[14] A. Modica, et al., J. Chem. Phys. 48 (1968) 3283.

[15] W. Jones, et al., J. Chem. Rev. 76 (1976) 563.